NANO LETTERS

pubs.acs.org/NanoLett

Letter

Halogen Electrochemistry Enabled Complementary Lithium/Halogen Dual-Ion Batteries with Enhanced Capacity and Cyclability

Kaiqiang Zhang, Qianchuan Yu, Jingjie Sun, Pengbo Zhang, Yaoda Wang, Yuge Feng, Zuoxiu Tie, and Zhong Jin*

Cite This: *Nano Lett.* 2025, 25, 16554−16563

Read Online

ACCESS | Metrics & More | Article Recommendations | Supporting Information

ABSTRACT: Rechargeable dual-ion batteries are promising supplements to lithium-ion batteries for fast charging and stationary energy storage but suffer from sluggish kinetics, low capacity, and poor durability caused by the insertion of bulky anions. Here, we introduce a halogen electrochemistry strategy employing small halogen ions as charge carriers to achieve efficient anion redox reactions. Among them, bromide ions exhibit superior electrochemical performances due to a suitable size and redox potential. The charge storage mechanisms involving Br^- intercalation (or adsorption) and conversion are demonstrated using graphite, a Co-terephthalic metal−organic framework (Co-BDC), and zeolitic imidazolate framework-67 (ZIF-67) as cathodes, delivering specific capacities of 197, 226, and 291 mAh g^{-1} at 100 mA g^{-1}, respectively. Electrochemical and spectroscopic analyses confirm that replacing large anions with small halogen ions brings enhanced ion storage capacities and redox kinetics. This work establishes halogen electrochemistry as a new paradigm for high-performance and scalable dual-ion secondary batteries.

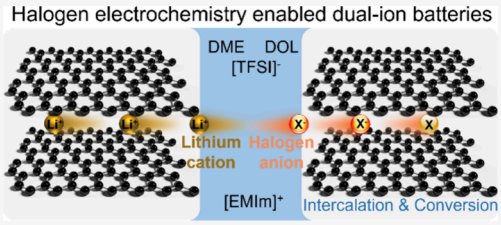

KEYWORDS: *Rechargeable Dual-Ion Batteries, Halogen Electrochemistry, Bromide Ions, Intercalation and Conversion Redox Reactions, Metal−Organic Frameworks, Electrochemical Energy Storage*

Dual-ion batteries, leveraging simultaneous and counter-directional migration of cations and anions, have emerged as an intriguing supplement to traditional lithium-ion batteries, promising enhanced fast-charging capabilities and extended cycle longevity.[1−4] During the charging process, cations undergo intercalation into the anodic host material, while anions concurrently intercalate into the cathodic host material. Conversely, upon discharging, the cations and anions deintercalate from their respective electrodes, reverting back to the electrolyte. These intertwined charge−discharge mechanisms are accompanied by electrode redox reactions, which play a pivotal role in the energy storage and release processes.[5−7] The distinctive charge storage mechanism in dual-ion batteries distinguish them from conventional lithium-ion batteries, which rely solely on cations as charge carriers traversing between anode and cathode.[8] This feature underscores the novelty and potential advantages of dual-ion batteries over their lithium-ion counterparts.

To date, the charging mechanism of dual-ion batteries predominantly entails the intercalation of anions into cathode materials, such as graphite and MoS_2.[9] However, the large size of traditional anion charge carriers (e.g., $[PF_6]^-$, $[HSO_4]^-$, and $[FSI]^-$) constrains the choice of cathodic host materials primarily to layered compounds featuring ample lattice spacings.[10−12] The intercalation of large anions renders the cathodic hosts prone to detrimental effects like delamination and pulverization, ultimately precipitating battery failure.[13,14] Moreover, the insertion of large anions necessitates a heightened operational voltage to surmount the steric hindrance.[15−18] The high voltage exacerbates the decomposition of the electrolyte, resulting in the formation of undesired byproducts at the cathode−electrolyte interface, which hinders the ion migration and increases the battery impedance.[19,20] In addition, contemporary dual-ion batteries reliant solely on intercalation reactions often exhibit a relatively modest capacity (~100 mAh g^{-1}). Recently, pioneering research has illuminated the superiority of conversion reactions over intercalation in bolstering charge storage capacity.[21,22] However, the design of innovative electrochemical redox systems that harmoniously integrate the intercalation (or adsorption) and conversion reactions of smaller charge carrier ions can address the persistent issues in dual-ion batteries.

Herein, we report the introduction of halogen electrochemistry in a dual-ion battery system by incorporating small halogen anions in the electrolytes for both intercalation (or adsorption) and conversion reactions to significantly boost battery capacity and cycle longevity. During the cycling

Received: October 2, 2025
Revised: October 30, 2025
Accepted: October 31, 2025
Published: November 6, 2025

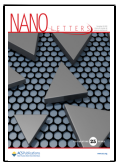

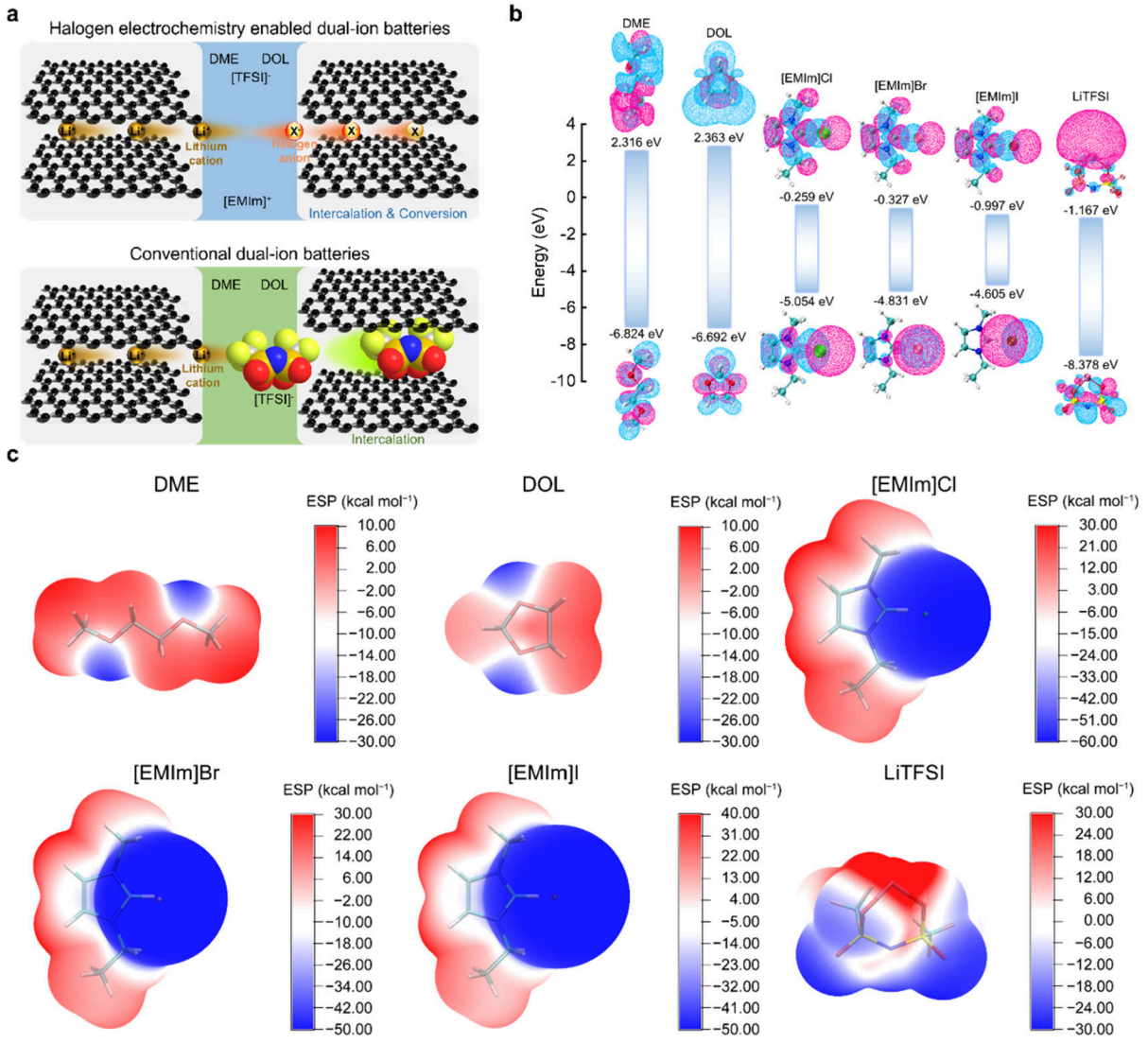

Figure 1. Schematic principle of halogen electrochemistry enabled complementary lithium/halogen dual-ion batteries. (a) Energy storage mechanism of dual-ion batteries based on (top) halogen electrochemistry and (bottom) conventional large anion intercalation. (b, c) Theoretical calculations of (b) HOMO/LUMO energies and (c) MESP for the chemicals used in the electrolytes.

processes, the small halogen ions efficiently intercalate (deintercalate) into (from) the interplanar spaces of the graphite electrode within a proper voltage range of 0−3 V (vs graphite electrode). Notably, halogen intercalation and conversion reactions were successfully incorporated into the charge storage process to facilitate capacity improvement. The combination of halogen electrochemistry with lithium intercalation/deintercation demonstrated good reversibility in as-fabricated graphite symmetric dual-ion batteries. To expand the range of cathodic host material options for complementary lithium/halogen dual-ion batteries, we also investigate halogen absorption by metal−organic frameworks (MOFs) and zeolitic imidazolate frameworks, both of which demonstrate stable adsorption and accommodation of halogen species during battery operation, enabling an almost 3-fold increase in capacity and a long cycling lifespan with high capacity retention. Beyond the lithium-based systems explored in this work, the proposed halogen electrochemistry concept has the potential to be extended to other cations, such as Na^+, K^+, etc. The relatively small ionic radii and tunable redox potentials of halogen ions (Cl^-, Br^-, and I^-) enable an efficient redox process across different electrolyte systems. Such versatility highlights the potential of halogen-based chemistry as a universal platform for developing next-generation rechargeable dual-ion batteries.

The proposed dual-ion batteries feature a two-step process involving intercalation and conversion during battery operation, contrasting with conventional batteries that solely rely on intercalation (Figure 1a). The intercalation of small halogen ions into layered host materials encounters less steric hindrance compared to large anions composed of multiple atoms, such as hexafluorophosphate ($[PF_6]^-$) and bis-(trifluoromethylsulfonyl)amide ($[FSI]^-$).[23−25] Therefore, the process requires a lower charging voltage to drive the process. Moreover, the incorporation of small halogen ions for intercalation into layered hosts expands the options of potential electrode materials, enriching the design possibilities for dual-ion batteries. Notably, the combined contribution of intercalation and conversion to energy storage capacity presents a viable solution for further enhancing the energy density over conventional dual-ion batteries.

https://doi.org/10.1021/acs.nanolett.5c04968
Nano Lett. 2025, 25, 16554−16563

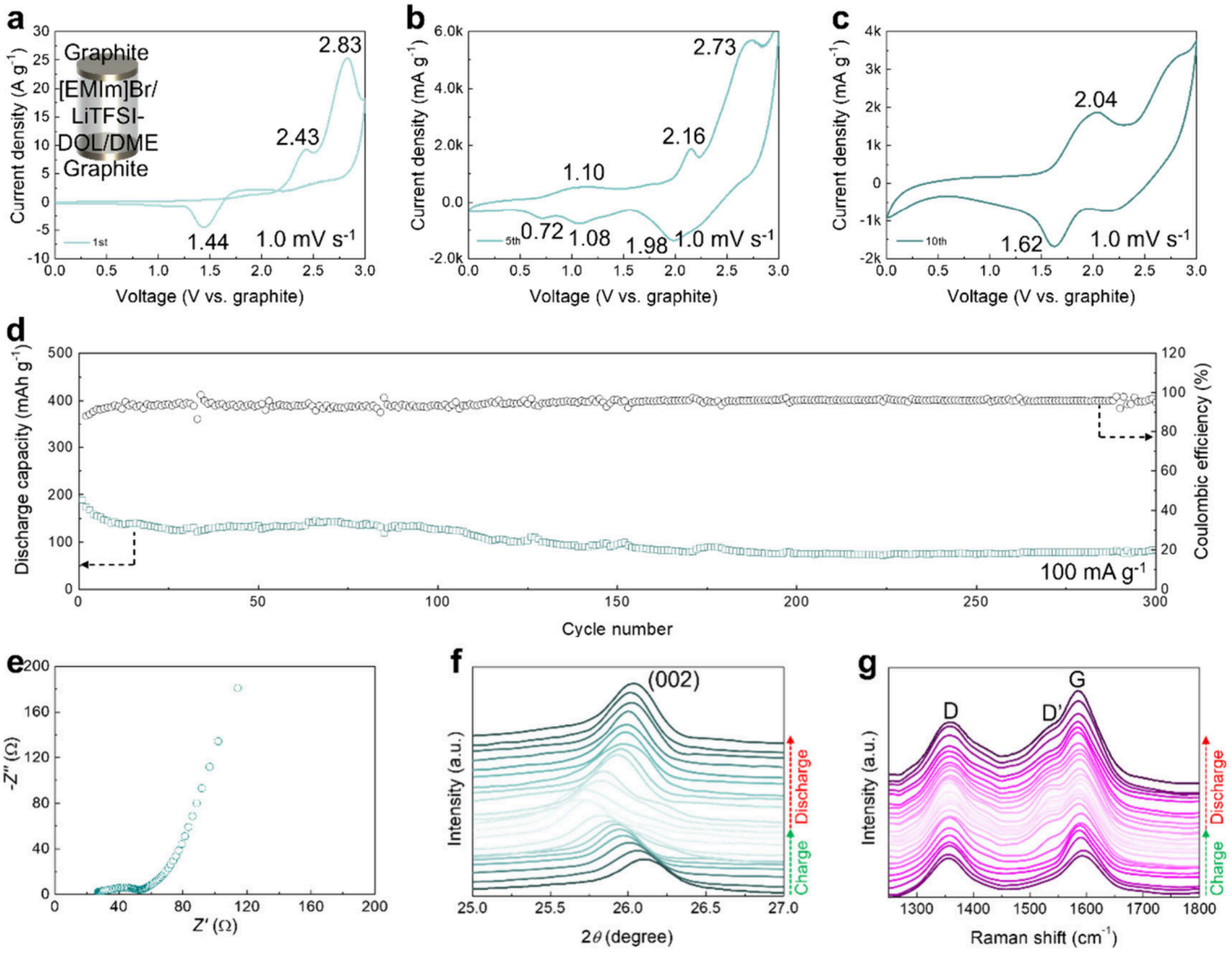

Figure 2. Electrochemical and spectroscopic analyses of the graphite||graphite dual-ion battery with Br^--containing electrolyte. (a–c) CV curves at various cycles, (d) galvanostatic cycling performance at a current density of 100 mA g^{-1}, and (e) EIS curves of the graphite||graphite dual-ion battery. Ex situ (f) XRD patterns and (g) Raman spectra of the graphite cathode during the charge–discharge processes.

The electrochemical stability of electrolyte solvents and solutes was assessed using molecular orbital theory by calculating the energies of the highest occupied molecular orbital (HOMO) and the lowest unoccupied molecular orbital (LUMO). The HOMO energy determines the ability to lose electrons (oxidation reaction), while the LUMO energy dictates the propensity to gain electrons (reduction reaction).[26,27] In theory, the energy gap between the HOMO and LUMO energy levels represents the voltage range that the chemical can withstand. Based on the theoretical calculations, the HOMO energy levels are determined to be −5.054 eV for 1-ethyl-3-methylimidazolium chloride ([EMIm]Cl), −4.831 eV for [EMIm]Br, −4.605 eV for [EMIm]I, −6.824 eV for dimethyl ether (DME), −6.692 eV for 1,3-dioxolane (DOL), and −8.378 eV for lithium bis(trifluoromethane)sulfonimide (LiTFSI) (Figure 1b). Additionally, we calculated the molecular electrostatic potential (MESP) of these compounds. The halogen species exhibited a concentrated region with a lower MESP value of approximately −50 kcal mol^{-1}, while the other chemical species showed distinct localized electronic distributions, reflecting significant molecular polarization (Figure 1c).

To demonstrate the concept of complementary lithium/halogen dual-ion batteries, we fabricated a graphite||graphite symmetric battery with a specially designed Br^--containing electrolyte, as detailed in the Methods section of the Supporting Information. The Fourier transform infrared (FTIR) spectroscopy analysis of the Br^--containing electrolyte revealed a superposition FTIR curve from the control samples of each component (Figure S1), indicating the compatibility of the introduced [EMIm]Br with the original electrolyte. To prevent electrolyte oxidation and promote redox reversibility, the charge cutoff voltage was set to 3.0 V (vs graphite electrode). Unless otherwise specified, all potentials are referenced to the respective anode used in each configuration (Li/Li^+ for Li||MOF cells and graphite for graphite-based cells). The potential of graphite is approximately 0.08–0.2 V higher than that of Li/Li^+, consistent with previous reports.[28,29] This representation was chosen to best reflect the actual device operation while enabling an approximate comparison between systems. Under the optimized operational conditions, the graphite||graphite symmetric battery exhibited redox peaks at 1.44, 2.43, and 2.83 V (vs graphite electrode, Figure 2a). Upon proceeding to the fifth cycle of CV scanning, redox peaks at 1.10, 2.16, 2.73, 0.72, 1.08, and 1.98 V (vs

https://doi.org/10.1021/acs.nanolett.5c04968
Nano Lett. 2025, 25, 16554–16563

graphite electrode) were observed (Figure 2b). The reversible redox peaks at 1.98 and 2.16 V (vs graphite electrode) are attributed to the charge storage processes of the graphite‖graphite symmetric dual-ion battery, while the other redox peaks are primarily ascribed to the activation process (Table S1). These redox processes eventually evolved into a single redox process situated at 1.62 and 2.04 V (vs graphite electrode, Figure 2c), suggesting the energy storage process in the graphite‖graphite dual-ion battery with Br^--containing electrolyte. During the continuous galvanostatic cycling tests, as shown in Figure 2d, the graphite‖graphite symmetric dual-ion battery with Br^--containing electrolyte delivered a capacity of 197 mAh g^{-1} at 100 mA g^{-1} and maintained 88.7 mAh g^{-1} after 300 cycles. This result confirmed that, by introducing small halogen ions into the electrolyte, the charge storage capacity was significantly improved compared to the conventional dual-ion batteries operating based on the intercalation and deintercalation of large anions.[30] Furthermore, the prepared graphite‖graphite symmetric dual-ion battery demonstrated a small charge transfer impedance of 25 Ω and an internal resistance of 30 Ω measured by electrochemical impedance spectroscopy (EIS) (Figure 2e). These results suggested that the incorporation of small Br^- ions into the conventional electrolyte for dual-ion batteries offered competitive electrochemical kinetics performance.[31]

Ex situ X-ray diffraction (XRD) analysis was used to investigate the processes of halogen ion intercalation into and deintercalation from the interstitial space of the graphite cathode in the graphite‖graphite dual-ion battery. During the charging process, as halogen intercalation progressed, the interplanar distance of graphite expanded as evidenced by the down-shift of the (002) peak in the XRD spectra (Figure 2f) according to the Bragg law ($2d \sin\theta = n\lambda$), where d represents the interplanar distance, θ is the diffraction angle, λ is the wavelength of the X-ray wave, and n is an integer.[32] Subsequently, the XRD spectra of the graphite‖graphite dual-ion battery exhibited an upshift of the (002) peak during the discharge process, indicating an interlayer deintercalation process of Br^- ions. The reversible (de)intercalation of Br^- ions into(from) the graphite electrode was also confirmed by monitoring the ex situ Raman spectra.[33,34] As shown in Figure 2g, the emergence of the D′ band during charging and its diminishment during discharging indicated the reversible lattice deformation of graphite during battery operation. These spectroscopic observations collectively verified that the halogen redox process proceeded through reversible structural evolution. It is worth noting that solvent co-intercalation may occur in graphite-based systems using ether-based solvents such as DME/DOL.[35,36] In the present halogen-ion-based electrolyte, limited co-intercalation of solvent molecules cannot be fully excluded. Nevertheless, the reversible spectroscopic results suggest that the graphite structure remains highly intact without noticeable disorder accumulation. These results indicate that potential solvent co-intercalation, if any, does not cause significant structural degradation or compromise the reversibility of halogen intercalation.

To further demonstrate the halogen conversion behavior during battery operation, we retrieved the graphite cathode in a graphite‖graphite dual-ion battery after charging and rinsed it with ethanol to dissolve the oxidized bromide species. The ethanol solution obtained from rinsing was subjected to ultraviolet−visible (UV−vis) absorption and Raman spectroscopy characterizations. The UV−vis spectrum showed distinct absorption peaks for the ethanol solution after rinsing (Figure S2a), indicating the oxidation of Br^- ions during battery charging. Typically, the UV−vis absorption spectra displayed two bands at approximately 250 and 320 nm, corresponding to the characteristic transitions of Br_3^-. In contrast, molecular Br_2 was reported to exhibit a single absorption near 410−420 nm. These qualitative results confirmed the occurrence of reversible halogen conversion. Additionally, the Raman spectrum of ethanol solution after rinsing exhibited the same signals of oxidized bromide species (Figure S2b,c). For visual confirmation of the Br^- oxidation reaction, a pouch cell with a transparent package was fabricated (as detailed in the Methods section of the Supporting Information). After the charging process was completed, the membrane of the pouch cell became pale-yellow, suggesting the production of oxidized bromide species (Figure S 2d). The Br^- oxidation was further confirmed in the graphite‖graphite battery with an increased Br^- electrolyte concentration of 5.0 M. After fully charging the battery, the ethanol solution obtained after rinsing the graphite cathode showed a bronzing color, and the formation of oxidized bromide species was confirmed by ex situ UV−vis absorption spectroscopy (Figure S2e,f). The concentration of [EMIm]Br substantially affects both the electrolyte properties and the halogen redox processes. Increasing the Br^- concentration from 1.0 to 5.0 M resulted in a stronger color transition from pale-yellow to bronze after charging, indicating a more pronounced oxidation of Br^- (Figure S2). Notably, a higher halide ion concentration enhances redox activity but also increases viscosity and reduces ionic conductivity.[37,38] In addition, the overall capacity in dual-ion systems depends on both the electrolyte compositions and the adsorption capacity of the electrode materials. Thus, optimizing the electrolyte concentration requires balancing the available active species with the electrode energy-storage capability. In this study, a higher [EMIm]Br concentration was primarily employed to emphasize the halogen conversion behavior as the color contrast provides direct experimental evidence for the redox reaction. These findings verified that reversible intercalation and conversion processes of Br^- ions occurred near the cathode−electrolyte interface during the cycling operation of the graphite‖graphite dual-ion battery.

Notably, layered cathode materials are usually prone to exfoliation due to the susceptibility of van der Waals force within the interplanar spaces.[39−41] To address this issue and enhance the electrochemical performance of lithium/halogen dual-ion batteries, we propose a battery design that replaces conventional layer cathode materials with metal−organic frameworks (MOFs). For this study, we synthesized and employed two typical MOF materials, namely, Co-terephthalic (Co-BDC) and zeolitic imidazolate framwork-67 (ZIF-67). These MOFs are characterized by strong coordination and covalent bonds, providing stable and robust cathodic host matrices.[42,43] The XRD patterns of the two MOFs agreed with the standard cards and previously reported XRD patterns (Figure S3).[44−47] Additionally, the Brunauer−Emmett−Teller (BET) measurements revealed micro- and mesoporous structures for Co-BDC and ZIF-67 (Figure S4), with pore volumes and specific surface areas of 0.028 $cm^3\ g^{-1}$ and 12.127 $m^2\ g^{-1}$ for Co-BDC and 0.609 $cm^3\ g^{-1}$ and 1027.422 $m^2\ g^{-1}$ for ZIF-67.

To demonstrate the strong absorption effect of MOFs for halogen species during battery charging, we fabricated Li‖Co-

https://doi.org/10.1021/acs.nanolett.5c04968
Nano Lett. 2025, 25, 16554−16563

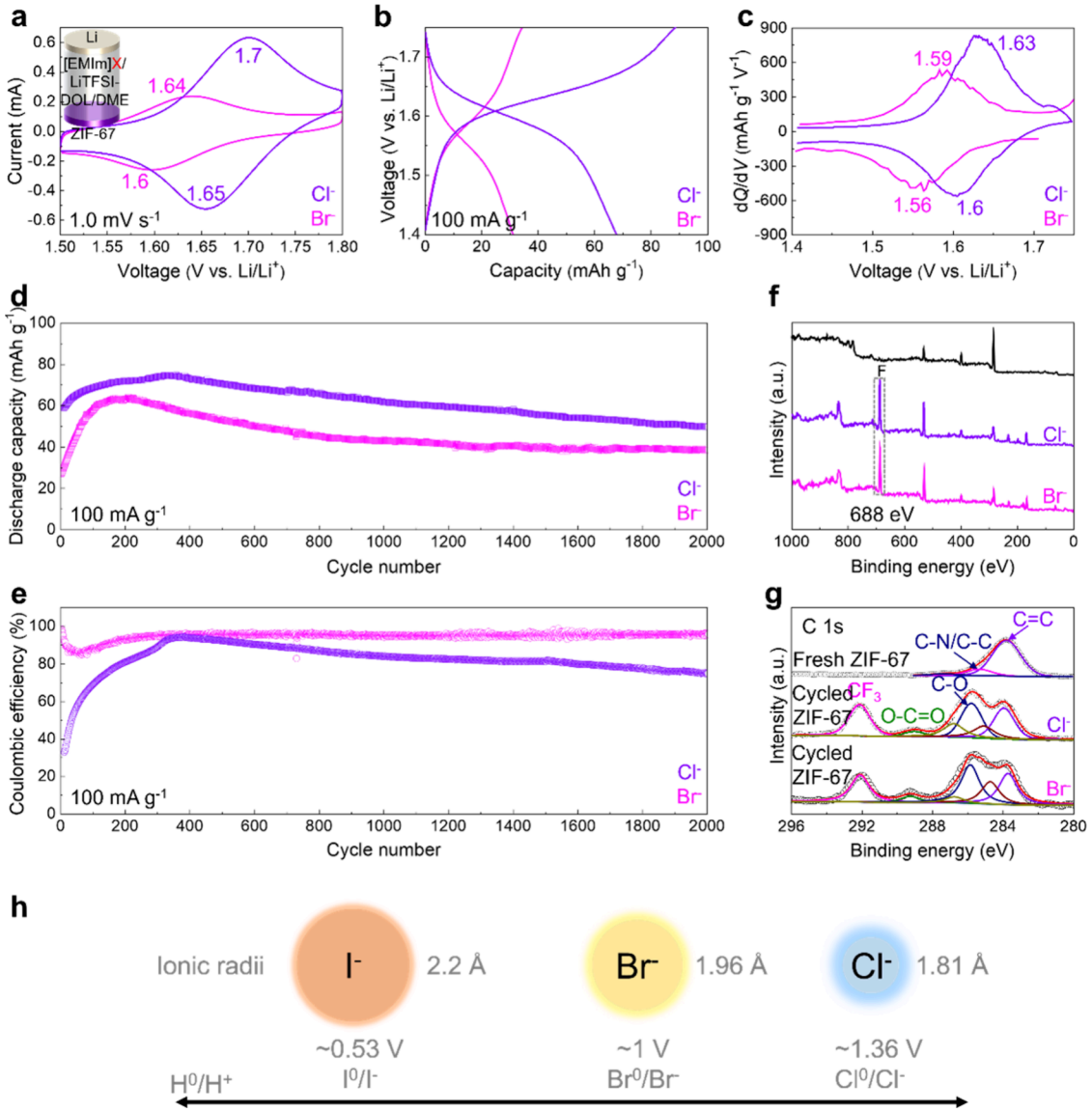

Figure 3. Electrochemical and spectroscopic characterizations of Li||ZIF-67 batteries with Cl^-- or Br^--containing electrolytes. (a) CV curves, (b) voltage profiles, (c) dQ/dV vs voltage plots, (d) capacity retention, and (e) Coulombic efficiency curves of Li||ZIF-67 batteries with Cl^-- or Br^--containing electrolytes, respectively. (f) Survey and (g) C 1s XPS spectra of the ZIF-67 cathode before and after cycling tests, respectively. (h) The correlations between halide ionic radii and redox potentials.

BDC and Li||ZIF-67 dual-ion batteries with Cl^--, Br^--, or I^--containing electrolytes. The CV curves of the Li||ZIF-67 dual-ion battery manifested a pair of redox peaks at 1.65 and 1.70 V (vs Li/Li^+) when using the Cl^--containing electrolyte and at 1.60 and 1.64 V (vs Li/Li^+) when using the Br^--containing electrolyte (Figure 3b). This redox pair persisted at 1.63 and 1.73 V (vs Li/Li^+) in the Li||Co-BDC dual-ion batteries with a Cl^--containing electrolyte and at 1.62 and 1.66 V (vs Li/Li^+) with a Br^--containing electrolyte (Figure S5a). The redox polarizations observed in Li||Co-BDC and Li||ZIF-67 dual-ion batteries with a Cl^--containing electrolyte (0.05 and 0.10 V) are larger if compared to those of the Br^--containing counterpart (0.04 and 0.04 V), which might be attributed to the larger electronic density of Cl^- anions. Notably, during the cycling processes of Li||Co-BDC and Li||ZIF-67 dual-ion batteries with Cl^-- or Br^--containing electrolytes, the voltage profiles exhibited a single voltage plateau (Figures 3c,d and S5b). However, the redox peaks were absent in Li||Co-BDC and Li||ZIF-67 dual-ion batteries with an I^--containing electrolyte, even when the voltage scanning range for CV curves was expanded (Figure S6), depicting a capacitive process. To further clarify the charge-storage mechanism, the reversible redox couples observed for both Cl^-- and Br^--containing electrolytes indicate that the reactions are dominated by halogen adsorption−intercalation rather than gas-phase halogen evolution. The electrochemical behaviors of halogen ions (Cl^-, Br^-, and I^-) are correlated with their ionic radii and standard redox potential. The smaller Cl^- ion (1.81 Å, E = 1.36 V vs H^0/H^+) exhibits stronger interaction with the host, leading to adsorption-dominated reactions with limited conversion contribution. The medium-sized Br^- ion (1.96 Å, E = 1. V vs H^0/H^+) enables balanced intercalation (or adsorption)−conversion reactions with enhanced capacity and reversibility. The larger I^- ion (2.2 Å, E = 0.53 V vs H^0/H^+) mainly undergoes conversion with larger polarization and lower Coulombic efficiency (Figure S6). These results

https://doi.org/10.1021/acs.nanolett.5c04968
Nano Lett. 2025, 25, 16554−16563

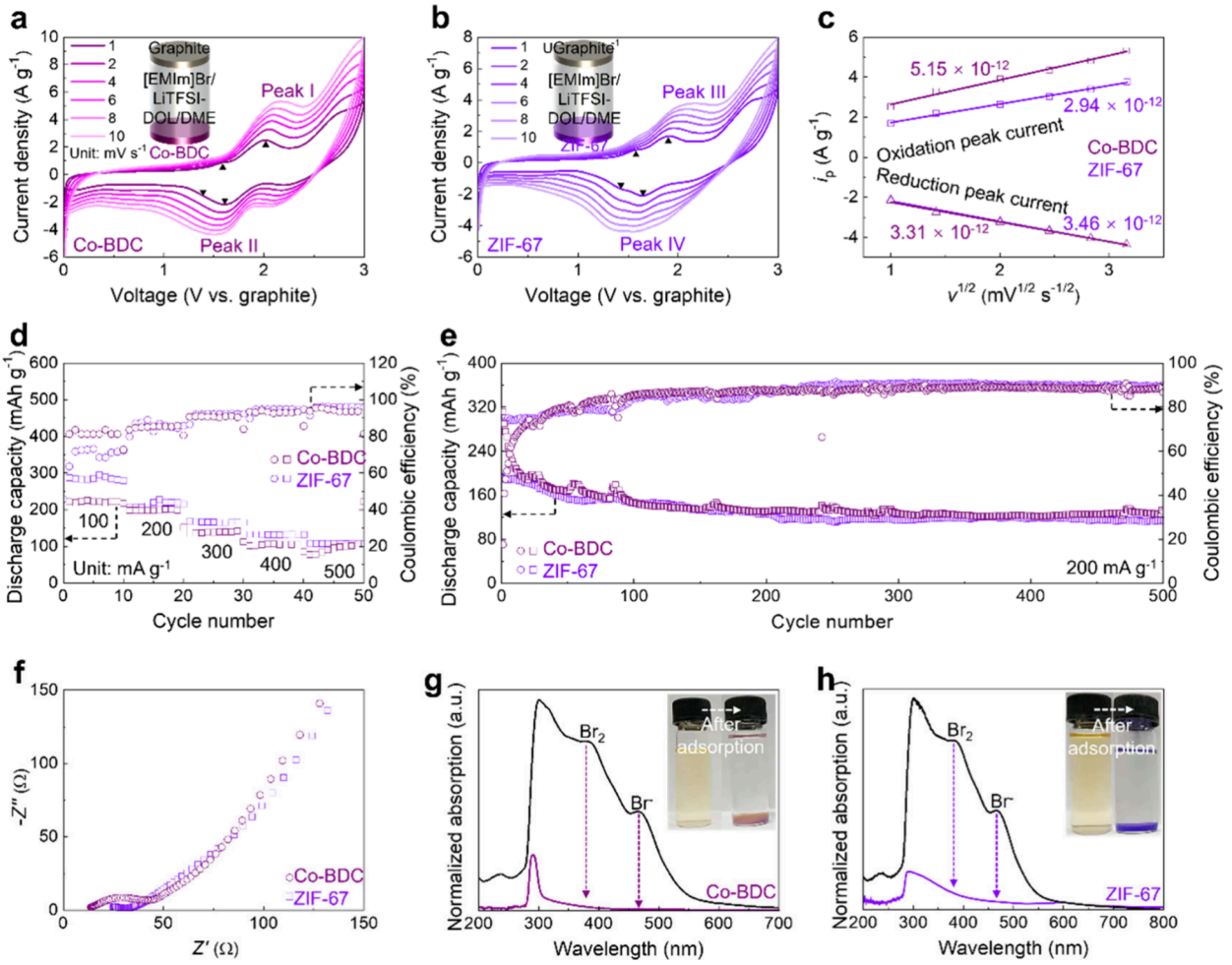

Figure 4. Electrochemical performances of graphite||MOF dual-ion batteries with a Br^--containing electrolyte. (a, b) CV curves, (c) i_p vs $\nu^{1/2}$ plots, (d) rate performances, (e) galvanostatic cycling tests, and (f) EIS curves for graphite||ZIF-67 and graphite||Co-BDC dual-ion batteries with a Br^--containing electrolyte. (g, h) UV−vis absorption spectra of a bromide ethanol solution before and after adsorption by (g) Co-BDC and (h) ZIF-67 powders. The insets in (g) and (h) show photographs of the bromide ethanol solutions before and after adsorption by the MOFs.

reveal that the balance between ion intercalation and conversion is governed jointly by the halide ionic size and redox potential, where moderate values yield the most efficient and reversible halogen electrochemistry.

To demonstrate the durability of MOF materials over the continuous adsorption and conversion of halogen ions, the Li|| Co-BDC and Li||ZIF-67 dual-ion batteries were subjected to galvanostatic cycling tests for 2000 cycles at 100 mA g^{-1}. When employing the Cl^--containing electrolyte, these batteries delivered higher initial capacities of 33.1 (for Li||Co-BDC) and 59.2 mAh g^{-1} (for Li||ZIF-67) compared to 19.1 (for Li|| Co-BDC) and 26.5 mAh g^{-1} (for Li||ZIF-67) with the Br^--containing counterpart (Figures 3e and S5c). However, the batteries utilizing the Br^--containing electrolyte enabled higher Coulombic efficiencies of 95.2% (for Li||Co-BDC) and 96.5% (for Li||ZIF-67) compared to 76.1% (for Li||Co-BDC) and 74.5% (for Li||ZIF-67) with the Cl^--containing counterparts (Figures 3f and S5d). Consequently, the Br^--containing electrolyte is proven to be more suitable for graphite||MOF dual-ion batteries. Throughout long-term cycling (up to 2000 cycles), the Li||Co-BDC batteries exhibited stable electrochemical performances and high capacity retention, particularly for the battery using a Cl^--containing electrolyte (Figure S5). Although no additional post-mortem characterizations were conducted, the maintained capacity confirms that the Co-BDC MOF remained structurally intact during the repeated halogenation/dehalogenation processes. In contrast, the Li|| ZIF-67 batteries exhibited a faster capacity decay (Figure 3e), suggesting lower compatibility with the halogenation environment. These results highlight the importance of structural stability and compatibility between MOF host materials and halogen-related electrochemical processes. Moreover, X-ray photoelectron spectroscopy (XPS) analysis of the ZIF-67 cathode after continuous cycling tests revealed the emergence of $-CF_3$ binding at 688 eV in the survey XPS spectra (Figure 3g) and at 292.1 eV in the deconvoluted C 1s XPS spectra (Figure 3h), suggesting the decomposition of $[TFSI]^-$ ions during the initial battery activation.

Following the demonstration of halogen absorption by the MOF host materials, we further fabricated graphite||MOF dual-ion batteries by utilizing a Br^--containing electrolyte. Both graphite||Co-BDC and graphite||ZIF-67 dual-ion batteries exhibited dual pairs of redox peaks, with the low-intensity redox peaks at a lower charge voltage corresponding to the electrochemical response of halogen absorption by MOFs. The high intensities of redox peaks suggested that the capacity value was primarily contributed by the halogen conversion processes (Figure 4a,b). The single merged reduction peak in

https://doi.org/10.1021/acs.nanolett.5c04968
Nano Lett. 2025, 25, 16554−16563

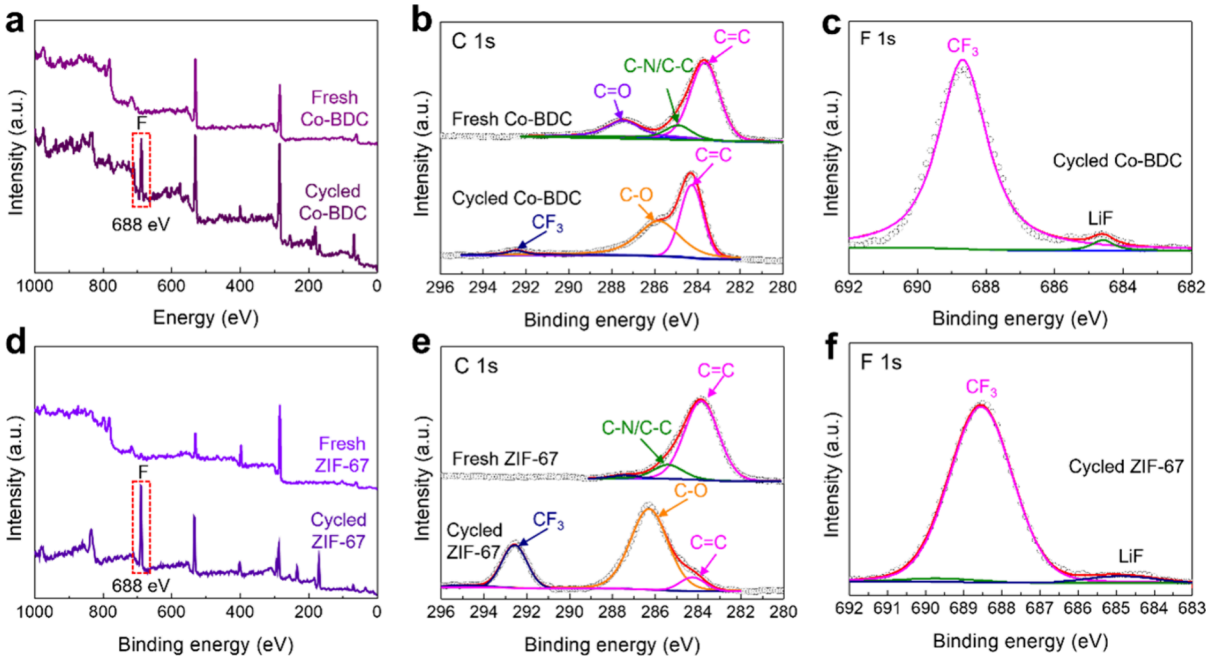

Figure 5. Ex situ characterizations of cycled MOF cathodes for analyzing the energy storage mechanism. (a, d) Survey XPS spectra, (b, e) deconvoluted C 1s XPS spectra, and (c, f) deconvoluted F 1s XPS spectra of (a–c) Co-BDC and (d–f) ZIF-67 cathodic hosts before and after cycling tests, respectively.

the CV curves of the graphite||Co-BDC dual-ion battery was observed due to the superposition of redox peaks (Figure 4a). The lower voltage plateaus were attributed to the adsorption/intercalation of halogen species, whereas the higher voltage plateaus originated from the subsequent conversion reactions. This two-step halogen redox process collectively contributed to the high capacity and cycling stability of the dual-ion secondary batteries. Furthermore, the diffusion coefficients were determined using the Randles–Ševčík equation ($I_p = 2.69 \times 10^5 n^{3/2} A C D^{1/2} \nu^{1/2}$), assuming $n = 1$ ($Br^- \rightarrow Br^0 + e^-$), $A = 1.13$ cm^2 (12 mm diameter electrode), and $C = 10^{-3}$ mol cm^{-3}. The linear relationships ($R^2 > 0.99$) between I_p and $\nu^{1/2}$ confirm diffusion-controlled kinetics. Considering uncertainties in geometric and fitting factors, the estimated diffusion coefficients have an overall uncertainty of ±15–20%.[48,49] The calculated diffusion parameters were 5.15×10^{-12} for peak I, 3.31×10^{-12} for peak II, 2.94×10^{-12} for peak III, and 3.46×10^{-12} for peak IV (Figure 4c).

Impressively, the graphite||ZIF-67 dual-ion battery delivered a high capacity of 291 mAh g^{-1} at 100 mA g^{-1}, significantly surpassing the capacity of conventional dual-ion batteries, which underscored the efficiency of the halogen-absorption- and conversion-based energy storage processes. After increasing the current density by a factor of 5, a capacity of 112 mAh g^{-1} was still maintained (Figure 4d). Similarly, the graphite||Co-BDC dual-ion battery delivered capacities of 226 and 101 mAh g^{-1} at 100 and 500 mA g^{-1}, respectively (Figure 4d). The voltage profiles of both batteries exhibited a distinct voltage plateau, indicating halogen adsorption and conversion processes (Figure S7a,b). The graphite||ZIF-67 dual-ion battery exhibited an initial capacity of 180 mAh g^{-1} at 200 mA g^{-1}, with a capacity retention ratio of 64% after 500 continuous cycles. The graphite||Co-BDC dual-ion battery exhibited an initial capacity of 190 mAh g^{-1} and a slightly higher capacity retention ratio of 67% after 500 cycles (Figure 4e). In addition, both the graphite||Co-BDC and graphite||ZIF-67 dual-ion batteries exhibited a low electrochemical impedance (~30 Ω for graphite||Co-BDC and 20 Ω for graphite||ZIF-67) as measured by EIS, which is conducive to high redox kinetics and rate performances for the batteries (Figure 4f).

Furthermore, the adsorption behaviors of MOF host cathodes toward oxidized bromide species were studied by conducting ex situ UV–vis absorption spectroscopy on the ethanol solution dissolved as-formed oxidized bromide species after battery charging. Initially, the UV–vis absorption spectra displayed prominent bromide absorption peaks, which gradually diminished after 8 h of MOF adsorption (Figure 4g,h). Accordingly, the colors of bromide ethanol solutions transformed from pale-yellow to a colorless and transparent appearance after adsorption by Co-BDC and ZIF-67 (insets in Figure 4g,h), confirming the effectiveness of Co-BDC and ZIF-67 for the adsorption and accommodation of oxidized bromide species.

To further reveal the effects of Br^--containing electrolytes on electrodes during battery operation, we conducted post-mortem characterizations using the XPS technique. Comparative survey XPS analyses between the fresh and cycled Co-BDC and ZIF-67 cathodes revealed a prominent F 1s XPS peak at ~688 eV (Figure 5a,d), which is consistent with the XPS spectra of the above-mentioned Li||MOF batteries (Figure 3f). The presence of the F element was further confirmed by the deconvoluted C 1s peak at 292.7 eV (Figure 5b,e) and F 1s peak at 688.5 eV (Figure 5c,f), which aligned with the survey XPS spectra. Moreover, a strong C–O bond at 296.5 eV was observed in the cycled MOF cathodes, suggesting the formation of a cathode–electrolyte interface (CEI) layer. In this dual-ion battery system, LiTFSI served as the exclusive source of F element. The above characterization results supported the decomposition of $[TFSI]^-$ anions and participation in the formation of the CEI layer on the cathode surface, consistent with previous reports.[50] Our theoretical

https://doi.org/10.1021/acs.nanolett.5c04968
Nano Lett. 2025, 25, 16554–16563

calculations of the HOMO and LUMO energy levels revealed that LiTFSI possessed the lowest HOMO energy level of −8.378 eV (Figure 1b). This activation process was also captured in the initial CV curves, showing several irreversible oxidation peaks at ∼2.5 V (Figure S7c,d). These oxidation peaks diminished after the initial activation, leaving behind only reversible redox peaks, as shown in Figure 4a,b. After this initial activation process in the dual-ion battery, the charge storage reaction dominated the subsequent cycles. Therefore, the formation of a fluorine-rich CEI layer stabilized the electrode−electrolyte interface during repeated charge−discharge redox reactions, mitigating side reactions and contributing to higher Coulombic efficiency during long-term cycling.

We developed a complementary lithium/halogen dual-ion battery system leveraging halogen electrochemistry, specially utilizing halogen adsorption and conversion reactions for energy storage applications. Among the tested halogen ions, Br^- anions exhibited superior electrochemical performances compared to Cl^- and I^- anions. The intercalation (or absorption) and conversion processes of Br^- anions demonstrated excellent reversibility, nearly tripling the capacity relative to conventional dual-ion batteries based on the (de)intercalation of larger anions. In addition, by incorporating Br^- anions into the electrolyte, this dual-ion battery design greatly broadens the range of viable cathodic host materials, as demonstrated by prototypical Co-BDC and ZIF-67 MOF materials. Overall, this study established halogen electrochemistry as a general and scalable strategy for advancing dual-ion battery technologies. The synergistic adsorption/intercalation-conversion mechanism, together with the abundance and low cost of halogen salts, offers new opportunities for constructing high-capacity, sustainable energy storage systems applicable to both lithium and non-lithium-based battery configurations.

■ ASSOCIATED CONTENT

Supporting Information

The Supporting Information is available free of charge at https://pubs.acs.org/doi/10.1021/acs.nanolett.5c04968.

Experimental details, Raman spectroscopy analyses, bromide oxidation behavior characterizations of the graphite||graphite dual-ion batteries with Br^--containing electrolyte, XRD characterizations of Co-BDC and ZIF-67 samples, BET analysis results of as-synthesized Co-BDC and ZIF-67, electrochemical characterizations of Li||Co-BDC dual-ion batteries with 1.0 M Cl^-- or Br^--containing electrolytes, CV curves and voltage profiles of Li||Co-BDC and Li||ZIF-67 dual-ion batteries with 1.0 M I^--containing electrolyte, voltage profiles and CV curves of graphite||Co-BDC and graphite||ZIF-67 dual-ion batteries with 1.0 M Br^--containing electrolyte (PDF)

■ AUTHOR INFORMATION

Corresponding Author

Zhong Jin − *State Key Laboratory of Coordination Chemistry, MOE Key Laboratory of Mesoscopic Chemistry, MOE Key Laboratory of High Performance Polymer Materials and Technology, Jiangsu Key Laboratory of Clean Energy Catalysis and Intelligent Green Chemical Engineering, Suzhou Key Laboratory of Green Intelligent Manufacturing of New Energy Materials and Devices, Tianchang New Materials and Energy Technologies Research Center, Institute of Green Chemistry and Engineering, School of Chemistry and Chemical Engineering, Nanjing University, Nanjing, Jiangsu 210023, P. R. China; School of Energy Sciences and Engineering, Nanjing Tech University, Nanjing, Jiangsu 211816, P. R. China;* orcid.org/0000-0001-8860-8579; Email: zhongjin@nju.edu.cn

Authors

Kaiqiang Zhang − *State Key Laboratory of Coordination Chemistry, MOE Key Laboratory of Mesoscopic Chemistry, MOE Key Laboratory of High Performance Polymer Materials and Technology, Jiangsu Key Laboratory of Clean Energy Catalysis and Intelligent Green Chemical Engineering, Suzhou Key Laboratory of Green Intelligent Manufacturing of New Energy Materials and Devices, Tianchang New Materials and Energy Technologies Research Center, Institute of Green Chemistry and Engineering, School of Chemistry and Chemical Engineering, Nanjing University, Nanjing, Jiangsu 210023, P. R. China; School of Energy Sciences and Engineering, Nanjing Tech University, Nanjing, Jiangsu 211816, P. R. China;* orcid.org/0000-0002-2288-4893

Qianchuan Yu − *State Key Laboratory of Coordination Chemistry, MOE Key Laboratory of Mesoscopic Chemistry, MOE Key Laboratory of High Performance Polymer Materials and Technology, Jiangsu Key Laboratory of Clean Energy Catalysis and Intelligent Green Chemical Engineering, Suzhou Key Laboratory of Green Intelligent Manufacturing of New Energy Materials and Devices, Tianchang New Materials and Energy Technologies Research Center, Institute of Green Chemistry and Engineering, School of Chemistry and Chemical Engineering, Nanjing University, Nanjing, Jiangsu 210023, P. R. China*

Jingjie Sun − *State Key Laboratory of Coordination Chemistry, MOE Key Laboratory of Mesoscopic Chemistry, MOE Key Laboratory of High Performance Polymer Materials and Technology, Jiangsu Key Laboratory of Clean Energy Catalysis and Intelligent Green Chemical Engineering, Suzhou Key Laboratory of Green Intelligent Manufacturing of New Energy Materials and Devices, Tianchang New Materials and Energy Technologies Research Center, Institute of Green Chemistry and Engineering, School of Chemistry and Chemical Engineering, Nanjing University, Nanjing, Jiangsu 210023, P. R. China*

Pengbo Zhang − *State Key Laboratory of Coordination Chemistry, MOE Key Laboratory of Mesoscopic Chemistry, MOE Key Laboratory of High Performance Polymer Materials and Technology, Jiangsu Key Laboratory of Clean Energy Catalysis and Intelligent Green Chemical Engineering, Suzhou Key Laboratory of Green Intelligent Manufacturing of New Energy Materials and Devices, Tianchang New Materials and Energy Technologies Research Center, Institute of Green Chemistry and Engineering, School of Chemistry and Chemical Engineering, Nanjing University, Nanjing, Jiangsu 210023, P. R. China*

Yaoda Wang − *State Key Laboratory of Coordination Chemistry, MOE Key Laboratory of Mesoscopic Chemistry, MOE Key Laboratory of High Performance Polymer Materials and Technology, Jiangsu Key Laboratory of Clean Energy Catalysis and Intelligent Green Chemical Engineering, Suzhou Key Laboratory of Green Intelligent Manufacturing of New Energy Materials and Devices, Tianchang New Materials and Energy Technologies Research Center, Institute*

https://doi.org/10.1021/acs.nanolett.5c04968
Nano Lett. 2025, 25, 16554−16563

of Green Chemistry and Engineering, School of Chemistry and Chemical Engineering, Nanjing University, Nanjing, Jiangsu 210023, P. R. China

Yuge Feng − *State Key Laboratory of Coordination Chemistry, MOE Key Laboratory of Mesoscopic Chemistry, MOE Key Laboratory of High Performance Polymer Materials and Technology, Jiangsu Key Laboratory of Clean Energy Catalysis and Intelligent Green Chemical Engineering, Suzhou Key Laboratory of Green Intelligent Manufacturing of New Energy Materials and Devices, Tianchang New Materials and Energy Technologies Research Center, Institute of Green Chemistry and Engineering, School of Chemistry and Chemical Engineering, Nanjing University, Nanjing, Jiangsu 210023, P. R. China*

Zuoxiu Tie − *State Key Laboratory of Coordination Chemistry, MOE Key Laboratory of Mesoscopic Chemistry, MOE Key Laboratory of High Performance Polymer Materials and Technology, Jiangsu Key Laboratory of Clean Energy Catalysis and Intelligent Green Chemical Engineering, Suzhou Key Laboratory of Green Intelligent Manufacturing of New Energy Materials and Devices, Tianchang New Materials and Energy Technologies Research Center, Institute of Green Chemistry and Engineering, School of Chemistry and Chemical Engineering, Nanjing University, Nanjing, Jiangsu 210023, P. R. China*

Complete contact information is available at: https://pubs.acs.org/10.1021/acs.nanolett.5c04968

Author Contributions

The manuscript was written through contributions from all authors. K.Z. and Q.Y. contributed equally to this work. Z.J. and K.Z. conceived the idea of this study. K.Z. and Q.Y. conducted the electrochemical and spectroscopic characterizations. J.S., P.Z., Y.W., Y.F., and Z.T. conducted the theoretical calculation and spectroscopic and visual experiments. All authors discussed the results and have given approval to the final version of the manuscript.

Notes

The authors declare no competing financial interest.

■ ACKNOWLEDGMENTS

The authors are grateful for the support from the National Natural Science Foundation of China (22561160129, 22479074, 22475096), the Equipment Pre-Research and Ministry of Education Joint Fund (8091B02052407), the Fundamental Research Program Key Project of Jiangsu Province (BK20253008), the Natural Science Foundation of Jiangsu Province (BK20221446, BK20240400, BK20241236), the Science and Technology Major Project of Jiangsu Province (BG2024013), the Scientific and Technological Achievements Transformation Special Fund of Jiangsu Province (BA2023037), the Academic Degree and Postgraduate Education Reforming Project of Jiangsu Province (JGKT24_C001), the Key Core Technology Open Competition Project of Suzhou City (SYG2024122), the Open Research Fund of Suzhou Laboratory (SZLAB-1308-2024-TS005), and the Chenzhou National Sustainable Development Agenda Innovation Demonstration Zone Provincial Special Project (2023sfq11).

■ REFERENCES

(1) Wang, M.; Tang, Y. A Review on the Features and Progress of Dual-Ion Batteries. *Adv. Energy Mater.* **2018**, *8* (19), 1703320.

(2) Placke, T.; Heckmann, A.; Schmuch, R.; Meister, P.; Beltrop, K.; Winter, M. Perspective on Performance, Cost, and Technical Challenges for Practical Dual-Ion Batteries. *Joule* **2018**, *2* (12), 2528−2550.

(3) Ou, X.; Gong, D.; Han, C.; Liu, Z.; Tang, Y. Advances and Prospects of Dual-Ion Batteries. *Adv. Energy Mater.* **2021**, *11* (46), 2102498.

(4) Zhang, L.; Wang, H.; Zhang, X.; Tang, Y. A Review of Emerging Dual-Ion Batteries: Fundamentals and Recent Advances. *Adv. Funct. Mater.* **2021**, *31* (20), 2010958.

(5) Zhou, X.; Liu, Q.; Jiang, C.; Ji, B.; Ji, X.; Tang, Y.; Cheng, H.-M. Strategies Towards Low-Cost Dual-Ion Batteries with High Performance. *Angew. Chem., Int. Ed.* **2020**, *59* (10), 3802−3832.

(6) Sui, Y.; Liu, C.; Masse, R. C.; Neale, Z. G.; Atif, M.; AlSalhi, M.; Cao, G. Dual-Ion Batteries: the Emerging Alternative Rechargeable Batteries. *Energy Storage Mater.* **2020**, *25*, 1−32.

(7) Hao, J.; Li, X.; Song, X.; Guo, Z. Recent Progress and Perspectives on Dual-Ion Batteries. *EnergyChem.* **2019**, *1* (1), 100004.

(8) Zhang, X.; Tang, Y.; Zhang, F.; Lee, C.-S. A Novel Aluminum-Graphite Dual-Ion Battery. *Adv. Energy Mater.* **2016**, *6* (11), 1502588.

(9) Wang, H.-G.; Wang, Y.; Wu, Q.; Zhu, G. Recent Developments in Electrode Materials for Dual-Ion Batteries: Potential Alternatives to Conventional Batteries. *Mater. Today* **2022**, *52*, 269−298.

(10) Zhu, H.; Zhang, F.; Li, J.; Tang, Y. Penne-Like MoS_2/Carbon Nanocomposite as Anode for Sodium-Ion-based Dual-Ion Battery. *Small* **2018**, *14* (13), 1703951.

(11) Li, C.; Lao, B.; Li, Z.; Yin, H.; Yang, Z.; Wang, H.; Chen, D.; Zhang, X.; Xu, Y.; Sun, C. Dual-Ion Battery with MoS_2 Cathode. *Energy Storage Mater.* **2020**, *32*, 159−166.

(12) Latha, M.; Rani, J. V. WS_2/Graphene Composite as Cathode for Rechargeable Aluminum-Dual Ion Battery. *J. Electrochem. Soc.* **2020**, *167* (7), 070501.

(13) Yang, H.; Qin, T.; Zhou, X.; Feng, Y.; Wang, Z.; Ge, X.; Yue, N.; Li, D.; Zhang, W.; Zheng, W. Boosting the Kinetics of PF_6^- into Graphitic Layers for the Optimal Cathode of Dual-Ion Batteries: the Rehearsal of Pre-Intercalating Li^+. *J. Energy Chem.* **2022**, *71*, 392−399.

(14) Liu, Y.; Deng, W.; Meng, Z.; Wong, W.-Y. A Tetrakis (Terpyridine) Ligand-based Cobalt(ii) Complex Nanosheet as a Stable Dual-Ion Battery Cathode Material. *Small* **2020**, *16* (17), 1905204.

(15) Rodríguez-Pérez, I. A.; Ji, X. Anion Hosting Cathodes in Dual-Ion Batteries. *ACS Energy Lett.* **2017**, *2* (8), 1762−1770.

(16) Kravchyk, K. V.; Bhauriyal, P.; Piveteau, L.; Guntlin, C. P.; Pathak, B.; Kovalenko, M. V. High-Energy-Density Dual-Ion Battery for Stationary Storage of Electricity Using Concentrated Potassium Fluorosulfonylimide. *Nat. Commun.* **2018**, *9* (1), 1−9.

(17) Das, S.; Manna, S. S.; Pathak, B. Recent Advancements in Devising Computational Strategies for Dual-Ion Batteries. *ChemSusChem* **2023**, *16* (4), No. e202201405.

(18) Yang, K.; Jia, L.; Liu, X.; Wang, Z.; Wang, Y.; Li, Y.; Chen, H.; Wu, B.; Yang, L.; Pan, F. Revealing the Anion Intercalation Behavior and Surface Evolution of Graphite in Dual-Ion Batteries via in situ AFM. *Nano Res.* **2020**, *13* (2), 412−418.

(19) Fan, L.; Liu, Q.; Chen, S.; Lin, K.; Xu, Z.; Lu, B. Potassium-based Dual Ion Battery with Dual-Graphite Electrode. *Small* **2017**, *13* (30), 1701011.

(20) Li, W.-H.; Liang, H.-J.; Hou, X.-K.; Gu, Z.-Y.; Zhao, X.-X.; Guo, J.-Z.; Yang, X.; Wu, X.-L. Feasible Engineering of Cathode Electrolyte Interphase Enables the Profoundly Improved Electrochemical Properties in Dual-Ion Battery. *J. Energy Chem.* **2020**, *50*, 416−423.

(21) Yang, C.; Chen, J.; Ji, X.; Pollard, T. P.; Lü, X.; Sun, C.-J.; Hou, S.; Liu, Q.; Liu, C.; Qing, T.; Wang, Y.; Borodin, O.; Ren, Y.; Xu, K.; Wang, C. Aqueous Li-Ion Battery Enabled by Halogen Conversion-Intercalation Chemistry in Graphite. *Nature* **2019**, *569* (7755), 245−250.

(22) Hou, S.; Chen, L.; Fan, X.; Fan, X.; Ji, X.; Wang, B.; Cui, C.; Chen, J.; Yang, C.; Wang, W.; Li, C.; Wang, C. High-Energy and Low-Cost Membrane-Free Chlorine Flow Battery. *Nat. Commun.* **2022**, *13* (1), 1281.
(23) Ji, B.; Zhang, F.; Wu, N.; Tang, Y. A Dual-Carbon Battery based on Potassium-Ion Electrolyte. *Adv. Energy Mater.* **2017**, *7* (20), 1700920.
(24) Tan, H.; Zhai, D.; Kang, F.; Zhang, B. Synergistic PF_6^- and FSI^- Intercalation Enables Stable Graphite Cathode for Potassium-based Dual Ion Battery. *Carbon* **2021**, *178*, 363−370.
(25) Shen, D.; Wang, M.; Chen, W. Halogen Makes Manganese Metal Batteries Rechargeable. *Nano Res. Energy* **2024**, *2*, No. e9120119.
(26) Chen, X.; Zhang, Q. Atomic Insights into the Fundamental Interactions in Lithium Battery Electrolytes. *Acc. Chem. Res.* **2020**, *53* (9), 1992−2002.
(27) Li, B.; Zhao, J.; Zhang, Z.; Zhao, C.; Sun, P.; Bai, P.; Yang, J.; Zhou, Z.; Xu, Y. Electrolyte-Regulated Solid-Electrolyte Interphase Enables Long Cycle Life Performance in Organic Cathodes for Potassium-Ion Batteries. *Adv. Funct. Mater.* **2019**, *29* (5), 1807137.
(28) Dahn, J. R.; Zheng, T.; Liu, Y.; Xue, J. S. Mechanisms for Lithium Insertion in Carbonaceous Materials. *Science* **1995**, *270* (5236), 590−593.
(29) Tarascon, J.-M.; Armand, M. Issues and Challenges Facing Rechargeable Lithium Batteries. *Nature* **2001**, *414* (6861), 359−367.
(30) Kumar, S.; Bhauriyal, P.; Pathak, B. Computational Insights into the Working Mechanism of the $LiPF_6$-Graphite Dual-Ion Battery. *J. Phys. Chem. C* **2019**, *123* (39), 23863−23871.
(31) Wei, Y.; Tang, B.; Liang, X.; Zhang, F.; Tang, Y. An Ultrahigh-Mass-Loading Integrated Free-Standing Functional All-Carbon Positive Electrode Prepared Using an Architecture Tailoring Strategy for High-Energy-Density Dual-Ion Batteries. *Adv. Mater.* **2023**, *35* (30), 2302086.
(32) Anemone, G.; Taleb, A. A.; Politano, A.; Kuo, C.-N.; Lue, C. S.; Miranda, R.; Farías, D. Setting the Limit for the Lateral Thermal Expansion of Layered Crystals via Helium Atom Scattering. Phys. *Chem. Chem. Phys.* **2022**, *24* (21), 13229−13233.
(33) Bradley, D. A.; Ee, L. S.; Nawi, S. N. M.; Sani, S. F. A.; Khandaker, M.; Alzimami, K.; Jambi, L.; Alqhatani, A. Radiation Induced Defects in Graphite. *Appl. Radiat. Isot.* **2022**, *182*, 110141.
(34) Efthimiopoulos, I.; Stavrou, E.; Umemoto, K.; Mayanna, S.; Torode, A.; Smith, J. S.; Chariton, S.; Prakapenka, V. B.; Goncharov, A. F.; Wang, Y. High-Pressure Phase of Cold-Compressed Bulk Graphite and Graphene Nanoplatelets. *Phys. Rev. B* **2023**, *107* (18), 184102.
(35) Ferrero, G. A.; Åvall, G.; Janßen, K.; Son, Y.; Kravets, Y.; Sun, Y.; Adelhelm, P. Solvent co-Intercalation Reactions for Batteries and Beyond. *Chem. Rev.* **2025**, *125* (6), 3401−3439.
(36) Sun, Y.; Åvall, G.; Wu, S.-H.; Ferrero, G. A.; Freytag, A.; Groszewicz, P. B.; Wang, H.; Mazzio, K. A.; Bianchini, M.; Baran, V.; Risse, S.; Adelhelm, P. Solvent co-Intercalation in Layered Cathode Active Materials for Sodium-Ion Batteries. *Nat. Mater.* **2025**, *24*, 1−9.
(37) Xu, K. Electrolytes and Interphases in Li-Ion Batteries and Beyond. *Chem. Rev.* **2014**, *114* (23), 11503−11618.
(38) Chen, X.; Zhang, Q. Atomic Insights into the Fundamental Interactions in Lithium Battery Electrolytes. *Acc. Chem. Res.* **2020**, *53* (9), 1992−2002.
(39) Yang, B.; Tamirat, A. G.; Bin, D.; Yao, Y.; Lu, H.; Xia, Y. Regulating Intercalation of Layered Compounds for Electrochemical Energy Storage and Electrocatalysis. *Adv. Funct. Mater.* **2021**, *31* (52), 2104543.
(40) Divya, M. L.; Lee, Y.-S.; Aravindan, V. Solvent co-Intercalation: an Emerging Mechanism in Li-, Na-, and K-Ion Capacitors. *ACS Energy Lett.* **2021**, *6* (12), 4228−4244.
(41) Stephenson, T.; Li, Z.; Olsen, B.; Mitlin, D. Lithium Ion Battery Applications of Molybdenum Disulfide (MoS_2) Nanocomposites. *Energy Environ. Sci.* **2014**, *7* (1), 209−231.
(42) Lv, X.-L.; Feng, L.; Wang, K.-Y.; Xie, L.-H.; He, T.; Wu, W.; Li, J.-R.; Zhou, H.-C. A Series of Mesoporous Rare-Earth Metal-Organic Frameworks Constructed from Organic Secondary Building Units. *Angew. Chem., Int. Ed.* **2021**, *60* (4), 2053−2057.
(43) Yuan, S.; Qin, J.-S.; Li, J.; Huang, L.; Feng, L.; Fang, Y.; Lollar, C.; Pang, J.; Zhang, L.; Sun, D.; Alsalme, A.; Cagin, T.; Zhou, H.-C. Retrosynthesis of Multi-Component Metal-Organic Frameworks. *Nat. Commun.* **2018**, *9* (1), 808.
(44) Wang, C.; Yang, F.; Sheng, L.; Yu, J.; Yao, K.; Zhang, L.; Pan, Y. Zinc-Substituted ZIF-67 Nanocrystals and Polycrystalline Membranes for Propylene/Propane Separation. *Chem. Commun.* **2016**, *52* (85), 12578−12581.
(45) Feng, S.; Bu, M.; Pang, J.; Fan, W.; Fan, L.; Zhao, H.; Yang, G.; Guo, H.; Kong, G.; Sun, H.; Kang, Z.; Sun, D. Hydrothermal Stable ZIF-67 Nanosheets via Morphology Regulation Strategy to Construct Mixed-Matrix Membrane for Gas Separation. *J. Membr. Sci.* **2020**, *593*, 117404.
(46) Cai, X.; Peng, F.; Luo, X.; Ye, X.; Zhou, J.; Lang, X.; Shi, M. Understanding the Evolution of Cobalt-based Metal-Organic Frameworks in Electrocatalysis for the Oxygen Evolution Reaction. *ChemSusChem* **2021**, *14* (15), 3163−3173.
(47) Li, Y.-N.; Wang, S.; Zhou, Y.; Bai, X.-J.; Song, G.-S.; Zhao, X.-Y.; Wang, T.-Q.; Qi, X.; Zhang, X.-M.; Fu, Y. Fabrication of Metal-Organic Framework and Infinite Coordination Polymer Nanosheets by the Spray Technique. *Langmuir* **2017**, *33* (4), 1060−1065.
(48) Li, D.; Dai, L.; Ren, X.; Ji, F.; Sun, Q.; Zhang, Y.; Ci, L. Foldable Potassium-Ion Batteries Enabled by Free-Standing and Flexible SnS_2@C Nanofibers. *Energy Environ. Sci.* **2021**, *14* (1), 424−436.
(49) Ren, X.; Zhao, Q.; McCulloch, W. D.; Wu, Y. MoS_2 as a Long-Life Host Material for Potassium Ion Intercalation. *Nano Res.* **2017**, *10* (4), 1313−1321.
(50) Kim, S.; Park, S. O.; Lee, M.-Y.; Lee, J.-A.; Kristanto, I.; Lee, T. K.; Hwang, D.; Kim, J.; Wi, T.-U.; Lee, H.-W.; Kwak, S. K.; Choi, N.-S. Stable Electrode-Electrolyte Interfaces Constructed by Fluorine- and Nitrogen-Donating Ionic Additives for High-Performance Lithium Metal Batteries. *Energy Storage Mater.* **2022**, *45*, 1−13.

https://doi.org/10.1021/acs.nanolett.5c04968
Nano Lett. 2025, 25, 16554−16563